International Journal of Remote Sensing
Vol. 29, No. 14, 20 July 2008, 4189–4205

Application of the multifractal microcanonical formalism to the detection of fire plumes in NOAA–AVHRR data

H. YAHIA*†, A. TURIEL‡, N. CHRYSOULAKIS§, J. GRAZZINI¶, P. PRASTACOS§ and I. HERLIN†

†INRIA, BP 105, 78153 Le Chesnay Cedex, France
‡Institut de Ciències del Mar – CMIMA (CSIC), Passeig Marìtim de la Barceloneta, 37-49, 08003 Barcelona, Spain
§Forth IACM (RAD), Vassilika Vouton, PO Box 1358, GR-71110, Heraklion, Crete, Greece
¶EC – DG JRC, IES/SDI, Via E.Fermi, 1, 21020 Ispra, Italy

(*Received 9 August 2006; in final form 23 June 2007*)

In this article it is shown that the multifractal microcanonical formalism (herein referred to as MMF) has strong potential for bringing new solutions to a known problem in the analysis of some remotely sensed datasets: the determination of fire plumes in NOAA–AVHRR data. It has been proven that NOAA–AVHRR data can be used to detect plumes caused by fire accidents of different kinds. This work builds on previous studies and uses the MMF to introduce novel methods for the determination of plumes. The MMF can be used to derive geometrical superstructures (like certain multifractal topological manifolds and most importantly the so-called reduced signals) that are able to deal with the multiscale properties of turbulent geophysical fluid flows. These multiscale properties make use of the spatial distribution of grey-level values in the datasets and they are used in conjunction with previous pixel-based descriptors to enhance the determination of plume pixels.

1. Introduction

In several studies satellite remote sensing acquisitions have been used for the detection of fire accidents, the determination of plumes, and the analysis of emitted aerosols for the quantification of gaseous smoke expelled in forest or industrial fire incidents (Cahoon *et al.*, 1999; Chrysoulakis and Cartalis, 2003; Chrysoulakis and Opie, 2004; Chu *et al.*, 1998; Li *et al.*, 2001; Flasse and Ceccato, 1996; Hashim *et al.*, 2004). Most fire detection and plume determination algorithms are basically pixel-based: they use the grey-level values of pixels corresponding to a satellite acquisition over an extended ground area; depending on the physical properties of the acquired radiations, they determine appropriate threshold values and classify the pixels accordingly. For example, many fire detection algorithms with NOAA–AVHRR data first determine potential fire pixels using simple thresholds, then try to refine the thresholds and eliminate other bodies associated to non-fire pixels: non-fire high-temperature surfaces, clouds, and some highly reflective surfaces. These

*Corresponding author. Email: Hussein.Yahia@inria.fr

International Journal of Remote Sensing
ISSN 0143-1161 print/ISSN 1366-5901 online
http://www.tandf.co.uk/journals
DOI: 10.1080/01431160701840174

algorithms may use simple spatial contextual information in the process, but they are basically pixel-based.

The research presented herein is taking place in the framework of the determination of plumes associated to fire incidents. It is intended to enhance the discrimination process between plume and non-plume pixels by using the spatial distribution of grey-level values over acquired areas in the following manner: we want to take into account the spatial characteristics of turbulent geophysical fluid flows and use these spatial characteristics in combination with multispectral information. Such an enhancement is needed because:

- The derivation of general thresholds in pixel-based methodologies is not an easy task.
- False alarms may still be present.
- In certain situations, fire incident plumes are difficult to distinguish from ordinary meteorological clouds.

The key observation is that the turbulent behaviour of plumes corresponding to fire incidents should be accessible in the channels in which the acquired data correspond to the spatial distribution of a physical intensive variable like temperature. Since we are interested in getting information about the turbulent character of plumes (in comparison, for instance, to meteorological cloud structures) we have to rely on signal processing multiscale analysis techniques powerful enough to capture the power-law behaviours found in turbulent phenomena (Arneodo *et al.*, 1995; Frisch, 1995). An indication of the usefulness of such an approach can be found in some recent studies (Grazzini *et al.*, 2006; Turiel *et al.*, 2005a); in these papers, phenomena of meteorological interest (precipitation, convection in tropical clouds) are characterized in METEOSAT acquired data, hence demonstrating the possibility of analysing turbulent behaviour in data at NOAA–AVHRR resolution. In general plumes occupy less spatial extent than convective clouds. Moreover, their formation process and radiative properties are not the same. However, many hours after an incident, plumes of different kinds (Chrysoulakis and Cartalis (2003), §1) undergo various dispersion dynamics (for instance, in the case of haze-like plumes, dispersion can be related to dominant winds over the area), and their spatial extension can become large. Consequently, we expect to find some of the plume turbulent behaviour in the NOAA–AVHRR acquisitions.

Since pixel-based threshold methods and classification schemes have proven to be useful in the determination of plumes associated to fire incidents, we use as a starting method the pixel-based analysis and classification scheme proposed by Chrysoulakis and Cartalis (2003) and Chrysoulakis and Opie (2004) and the use of the multifractal microcanonical formalism (MMF) is intended to enhance that algorithm by providing new spatially-defined operators to help the discrimination process. Fire incidents may be of various origins, nevertheless it is reasonable to assume that the plumes recorded by the sensors are acquisitions of atmospheric fluids in the regime of fully developed turbulence (FDT). In this regime, it is now well known that there exists a fundamental connection between the multifractal hierarchy associated to turbulence and the spectrum of *singularity exponents* observed in the structure functions (Arneodo *et al.*, 1995). Satellite sensors have different spatial resolutions, consequently the determination of multiscale features may help the matching of turbulent structures between sensors of different resolutions.

The novel approach presented in this work hinges on the following points:

- We apply the MMF for analysing turbulent data. Doing so, we determine the singular exponents of NOAA–AVHRR acquisitions and derive a spatial structure from them, the Most Singular Manifold (abbreviated herein MSM); the MSM displays a multifractal behaviour.
- We set up a synthesized signal, the *multispectral reduced signal*, using a reconstruction formula which consists in diffusing multispectral gradient values, starting from the set of pixels defined by the MSM, over the whole image domain.

The basic idea of this paper is to perform the diffusion of gradients observed in certain NOAA–AVHRR spectral bands on the MSM, which is a geometric superstructure computed in the thermal infrared acquisition range: the multispectral reduced signal is a synthesized signal computed from multispectral information, but at the precise spatial locations of the MSM, because that latter structure records the positions of the the sharpest transitions in a turbulent geophysical fluid. As a result, a new method for discriminating plumes from other acquired bodies (clouds, water, etc.) is introduced, and it can be used in conjunction with purely pixel-based algorithms.

The article is organized in the following way. In §2 we review the pixel-based approach developed by Chrysoulakis and Cartalis (2003) and Chrysoulakis and Opie (2004), the physical characteristics of the NOAA–AVHRR data, and we present the datasets used in this study. The MMF is reviewed in §3, which introduces the singular exponents and the geometric superstructures that can be derived from it. The notion of multispectral reduced signal, which is central to this study, is presented and we explain how it can be used in relation with plumes. In §4 we present the methodology used in this work and the results obtained. We then explain how the MMF can be used in conjunction with pixel-based algorithms for better plume determination in remotely sensed data.

2. Acquired data and previous work

2.1 *NOAA–AVHRR data*

The data we use are NOAA–AVHRR images of the following acquisitions:

(1) A large plume development caused by a fire on a large oil tanker near Genoa, Italy, that occurred on April, 13, 1991.
(2) The plume associated to a forest fire in Guadalajara, Spain, in July 2005.
(3) The plumes generated over Baghdad after the bombings of that city in 2003.

The datasets feature the usual NOAA–AVHRR resolution of $1.1\,\text{km} \times 1.1\,\text{km}$ at the nadir, and a swath coverage up to 2700 km. The temporal components of each dataset are different:

(1) one temporal acquisition for the first dataset;
(2) ten temporal acquisitions for the second dataset;
(3) eight temporal acquisitions for the third dataset.

Note that for a given event, all the temporal acquisitions are not always exploitable, due to errors or artifacts in the acquisition process. For each temporal acquisition, the five NOAA spectral channels are available: channel c_1 in the visible

range (0.58–0.68 μm), c_2 in the near infrared range (0.72–1.10 μm), c_3 in the mid-infrared range (3.55–3.93 μm), c_4 (10.5–11.3 μm) and c_5 (11.5–12.5 μm) in the thermal infrared range.

Datasets used in this research are NOAA Level 1-b data with a dynamic range on 10 bits (1024 grey-level values). Images are geometrically corrected and calibrated, with grey-level values converted into brightness temperatures values (infrared bands c_3, c_4 and c_5), and reflectance values (c_1 and c_2 bands). A common projection system is used for the four datasets. We present, in figure 1, the five images corresponding to the Genoa acquisition in the five spectral bands available in NOAA–AVHRR acquisitions.

In the visible range, a plume reflectance is a function of the aerosol particle optical thickness (their size distribution) and of its liquid water content. In the thermal infrared range, a plume reflectance possesses a signature as it contains particles radiating as grey bodies. Fire in itself emits thermal radiation with a peak in the mid-infrared region, in accordance with the classical theory of blackbody radiation. Meteorological clouds have a strong reflectivity in the visible and near infrared bands. Water bodies strongly absorb radiations in the near infrared. The turbulent behaviour of fire plumes is mainly accessed in the thermal infrared bands of the electromagnetic spectrum, where the acquired data correspond to the spatial distribution of temperature, an intensive thermodynamical variable.

2.2 *Previous work*

In (Chrysoulakis and Cartalis, 2003; Chrysoulakis and Opie, 2004), and from the observation of the radiative properties of different bodies (meteorological clouds, water, vegetation, soil and, of course, plumes) in the NOAA–AVHRR spectral bands, two basic indices are introduced: NDVI and CLD:

$$\begin{aligned} \mathrm{NDVI} &= (r_2 - r_1)/(r_2 + r_1) \\ \mathrm{CLD} &= (r_5 - r_1)/(r_5 + r_1). \end{aligned} \tag{1}$$

In the definitions of these indices, r_i corresponds to grey-level values of channel c_i after the radiometric calibration has taken place (i.e. values are either brightness temperatures or reflectance values, in their respective units). Using the properties of clouds in the visible and infrared domains (high reflectance values, low top temperatures), likely behaviour of the plume counterparts and direct inspection of CLD histograms, a first threshold can be derived to roughly classify pixels associated to clouds and pixels associated to plumes. The NDVI then applies on a datset masked with a CLD threshold as before and tends to discriminate land pixels, plume pixels and water pixels. The algorithm is calibrated on a particular dataset, and a 2D feature space is defined with the previous indices. A pseudo-coloured image is defined in RGB colour space: (CLD, NDVI, 0) providing a new dataset in which the detection plumes is made easier.

In this study, we want to explore a different and new direction of research: we make use of the spatial information to analyse turbulence in the acquired data, and we try to enhance the discrimination process by the determination of different turbulent characteristics between plumes and other bodies. As a consequence, we compute a synthesized signal, called the multispectral reduced signal (and formally defined in §3.3) which is given as an input to the previous pixel-based method. The use of NOAA–AVHRR acquisition datasets is particularly meaningful in such a

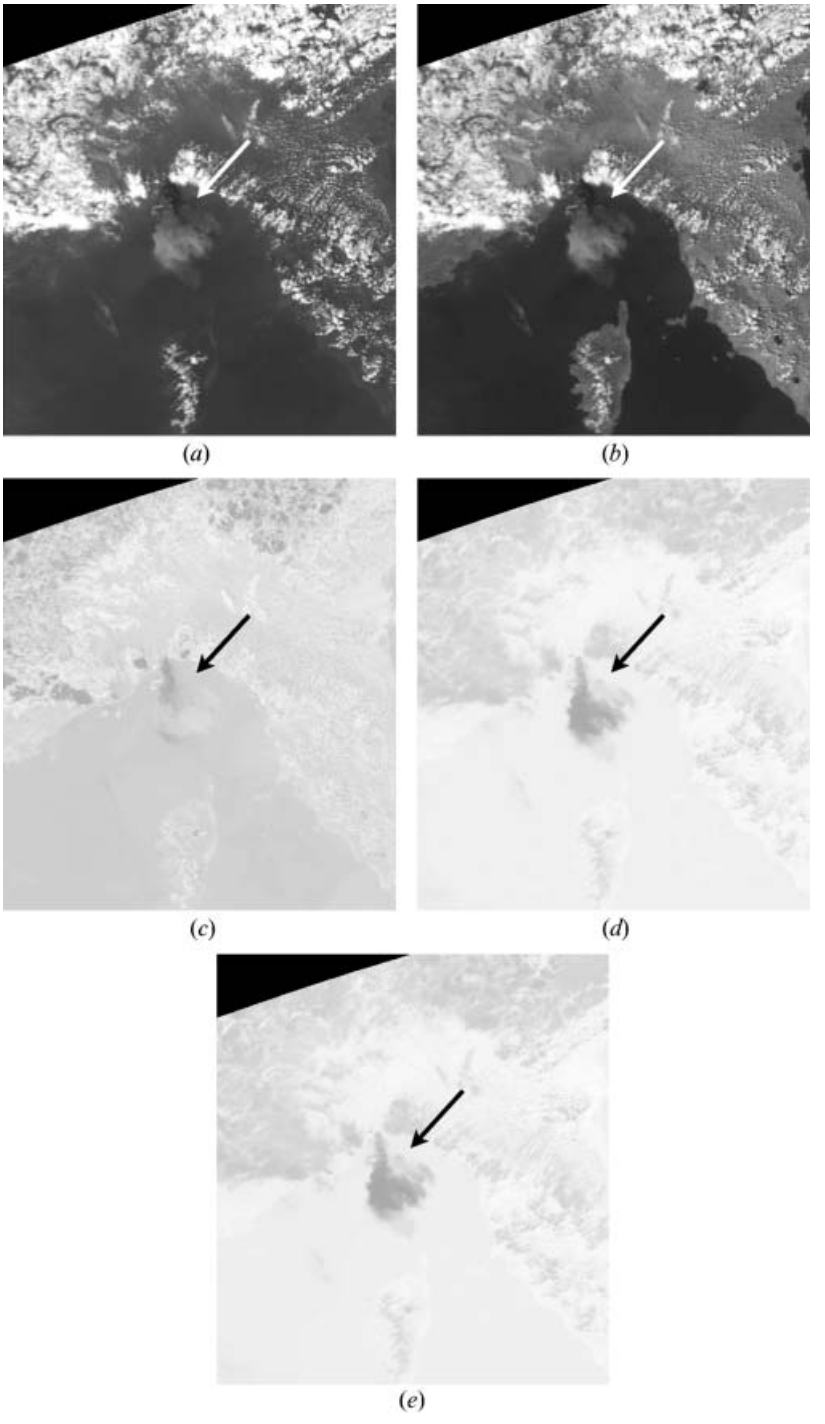

Figure 1. Images corresponding to the NOAA–AVHRR acquisitions of the Genoa accident, channels c_1 *(a)*, c_2 *(b)*, c_3 *(c)*, c_4 *(d)* and c_5 *(e)*. There is one large plume with non-uniform grey-level distribution of pixel values inside it (channels c_1, c_2). The plume is denoted by the white arrow in the first two channels, and by the black arrow in the others. In the thermal infrared bands c_4 and c_5, there is a non-uniform distribution of the plume's grey level values.

context: in the thermal bands, the acquired signal is related to the temperature of some atmospheric layers, which follows the complicated patterns typical of FDT (Fully Developed Turbulence, Roux *et al.* (2000)). In the context of FDT, one can expect any intensive physical quantity to be associated with multifractal structures (Parisi and Frisch, 1985; She and Levêque, 1994). We use the MMF to compute singularity exponents (see §3.1) associated to a multifractal measure defined on the acquired data. The singularity exponents describe the complex geometrical arrangement of the streamlines, they decompose the acquired signal into a hierarchy of geometric superstructures associated to the transition strength in the observed phenomena, and can be used to derive the statistical complexity of the underlying process (Turiel and Parge, 2000). We focus the analysis on one of these geometric superstructures, the MSM, defined as the subsets of data points having the lowest singular exponent, i.e. associated to the sharpest transitions. We will try to discriminate the differences between turbulent bodies by studying a synthesized signal computed with a universal diffusion kernel; the diffusion process is defined along the MSM, as the MSM contains the main geometrical information linked to turbulence, but we study the diffusion of different radiative or reflectance quantities along the MSM, allowing for the generation of a synthesized multspectral reduced signal; in the next section, we describe in more detail the MMF and the definition of the geometric structures associated to the singular exponents.

3. The microcanonical multifractal formalism and geometric superstructures

3.1 *Singularity exponents and most singular manifolds*

Let s be a geophysical signal (a NOAA–AVHRR acquisition in our case) defined over Ω, the signal's domain. The MMF allows the determination, at each point $\boldsymbol{x}$ in the signal's domain, of a *singular exponent* $h(\boldsymbol{x})$; the singular exponent describes the local irregularity of the signal around $\boldsymbol{x}$, and it is independent of the scale of study r. The reader is referred to Turiel and del Pozo (2002); Grazzini *et al.* (2002, 2006); Turiel *et al.* (2005a,b); Turiel and Parga (2000) for a description of the theoretical aspects and computational algorithms used in the MMF. The singular exponents computed in the framework of the MMF are good approximations of the power-law behaviour of thermodynamic observables in a geophysical turbulent flow. These exponents define a multifractal hierarchy of geometrical sets (the *geometric superstructures*) which is believed to be closely related to the flow dynamics (Turiel *et al.*, 2005b). Although some mathematical models of stochastic processes that simulate the generation of the exponents may lead to unbounded exponents (universal multifractals generated by stable laws) (Schertzer and Lovejoy, 1997), we assume that the spectrum of singularities (i.e. the set of all values $h(\boldsymbol{x})$) is bounded, as experimentation shows, and also because there are models, for instance with Log-Poisson multiplicative cascades, that offer adequate simulations of turbulence and produce a bounded spectrum of such exponents (Grazzini *et al.*, 2002). Consequently there is a lower bound $h_\infty = \inf\{h(\boldsymbol{x}), \boldsymbol{x} \in \Omega\}$ and an associated Most Singular Manifold F_∞:

$$\mathrm{F}_\infty = \{x \in \Omega | h(x) = h_\infty\}. \tag{2}$$

This set is defined by the points where the sharpest transitions occur in the signal, where the strength of the transition is defined by the value of the exponents. This notion of transition generalizes the classical notions of 'edge' encountered in image

processing, as it may capture transitions of any order, not only of integer type (corresponding to integer derivative discontinuities). The MSM can be oriented by computing the scalar product between the signal's gradient and a geometric vector field, orthogonal to the MSM. This geometric vector field is computed by diffusion of the MSM in an orthogonal direction using a simple radial nonlinear filter in Fourier space. We show in figure 2 the oriented MSM corresponding to the Genoa fire event, computed on thermal channel c_5 of the NOAA–AVHRR acquisition. In the next subsection, we develop the physical signification of the MSM, by showing that, even in the case of turbulent signals, it records almost all the information content associated to the acquisition. To do so, we make use of a reconstruction formula that will play a key role in the detection of plumes.

3.2 *The reconstruction formula*

Since the MSM contains the pixels where strongest transitions appear, an evident guess is the existence of a universal propagator that would permit the reconstruction of a whole signal from its values restricted to the MSM only. The propagator and the associated reconstruction formula are defined by the following equation in Fourier space (Turiel and del Pozo, 2002):

$$\widehat{s}(\boldsymbol{f}) = \frac{\sqrt{-1}\boldsymbol{f}\cdot\widehat{\nabla|_{\mathrm{F}_\infty} s}(\boldsymbol{f})}{\|\boldsymbol{f}\|^2} \tag{3}$$

where:

- $\boldsymbol{f}=(f_x, f_y)$ is the two-dimensional frequency vector;
- the hat symbol $\widehat{s}$ refers to the Fourier transform;
- $\nabla|_{\mathrm{F}_\infty} s$ is the signal's gradient restricted to the MSM;
- the dot symbol $\cdot$ in formula (3) refers to the vector dot product.

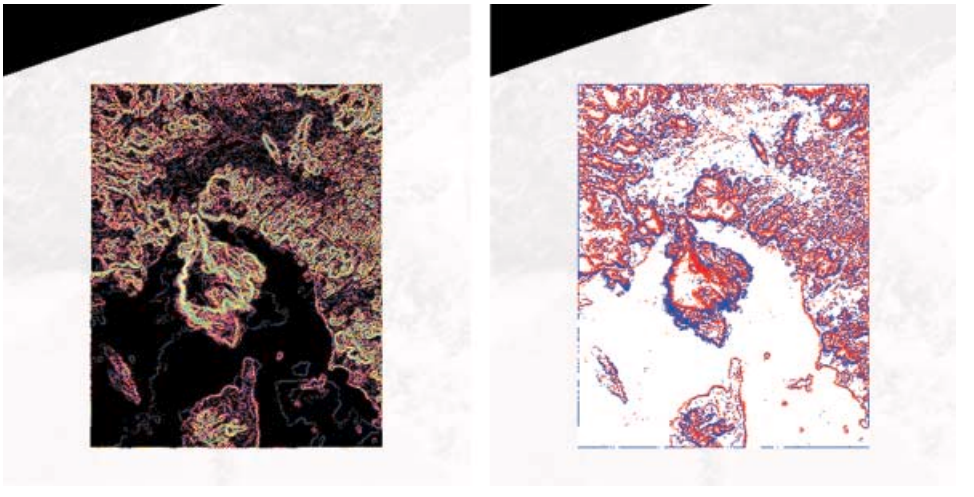

Figure 2. Left: visualization in false colours of the singularity exponents, computed on a selected rectangular area around the incident. The singular exponents are those of channel c_5 in the NOAA–AVHRR dataset (temperature). Note that the plume is well visible in the image of the exponents. Right: the MSM computed and visualized with two colours, corresponding to an orientation given by the signal's gradient (blue: positive orientation, red: negative).

In other words, the reconstruction process consists in propagating gradient values from the MSM to the whole image domain. The universal propagator, defined in Fourier space by

$$\widehat{g}(\boldsymbol{f}) = \frac{\sqrt{-1}\boldsymbol{f}}{\|\boldsymbol{f}\|^2}, \tag{4}$$

is the simplest propagator corresponding to the power spectrum of a translational invariant signal, a well known requirement for natural images (Turiel and del Pozo, 2002). Consequently, the reconstruction formula acts as a diffusion kernel propagation of gradient values from the MSM. If the MSM does encode the sharpest transitions, which correspond to the most informative content parts, the reconstruction formula should provide a good reconstruction of the original signal from its MSM. This is illustrated in figure 3.

The reconstruction formula allows us to reconstruct with great accuracy a whole turbulent signal with the knowledge of that signal on the most singular component only. The key idea of this article is introduced in the next subsection: we use the reconstruction formula (3) to compute a synthetic signal built from the MSM of the thermal infrared band, but with gradient values coming from the other channels of the NOAA–AVHRR acquisitions.

3.3 *The derivation of the synthesized multispectral reduced signal*

In the analysis of turbulent signals in the MMF, the MSM must be computed with the acquisition of a physical thermodynamical variable under the FDT regime. As explained in the previous sections, in the case of NOAA–AVHRR acquisitions, thermal infrared bands c_4 and c_5 are the best candidates. In this study, we make use of the c_5 band for the computation of the MSM: use of the c_4 band leads to similar results, and the two thermal infrared bands can be used interchangeably for the computation of the MSM.

We use the assumption that the MSM computed in the thermal infrared band is directly related to the streamlines of the underlying fluid, so we take this set as the correct reference on the geophysical fluid flow dynamics. Consequently, we want to use the information of the MSM in combination with other spectral bands to

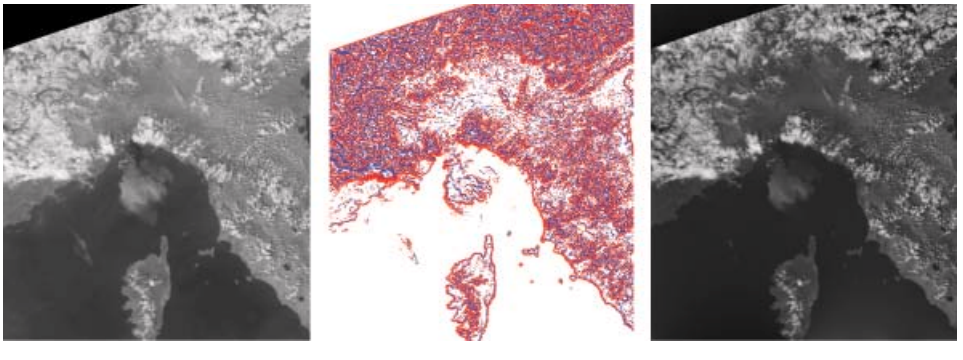

Figure 3. Left: channel c_2, NOAA–AVHRR acquisition of the fire accident near Genoa. Middle: the oriented MSM. Right: result of the reconstruction process. The MSM records the sharpest transitions in the signal, corresponding to the most informative parts in the signal. The right image is normalized.

provide a spatially-based discrimination method for the determination of plumes. We will use the signal gradient of a function of channels c_2 and c_3 to enhance the discrimination between plumes and others bodies taking into account temperature and reflectance information. Indeed, although the aerosol scattering effect in AVHRR channel 1 is larger than channel 2, reconstruction using channels 2 and 3 leads to better results with respect to non-plume bodies. Let $\varphi(c_2, c_3)$ be a function of the pixel's grey-level values acquired in spectral bands c_2 and c_3. We define a synthesized signal p by propagating φ's gradient vectors from the MSM computed in channel c_5; that is, we use the reconstruction formula (3) in which the gradient information is replaced by φ's gradient values $\nabla\varphi$:

$$\widehat{p}(\boldsymbol{f}) = \frac{\sqrt{-1}\boldsymbol{f}\cdot\widehat{\nabla|_{\mathrm{F}_\infty}\varphi}(\boldsymbol{f})}{\|\boldsymbol{f}\|^2} \tag{5}$$

which means that the gradient of φ is diffused from the set of strongest transitions on the thermal infrared channel. The algorithm is then as follows:

(1) Compute the singular exponents of the acquired signal s using wavelet decomposition in the thermal infrared band c_5.
(2) Derive the MSM F_∞ from the singular exponents by selecting pixels whose exponents are in a given fixed interval centred around the lowest exponent.
(3) Compute the gradient values $\nabla\varphi$ and set these values to zero outside F_∞ to get the singular gradient values $\nabla|_{\mathrm{F}_\infty}\varphi$.
(4) Compute the synthesized signal $\widehat{p}(f)$ in Fourier space using equation (5).
(5) Determine the synthesized signal p in spatial coordinates by use of the inverse Fourier transform.

The resulting synthesized signal p is called a multispectral reduced signal in the following. The determination of a universal φ function is still a subject of research. At this point of the work, we propose reasonable choices in §4 below.

4. Experiments and results

In this section, we apply the model and compute the synthesized multispectral reduced signals on each dataset.

4.1 *Genoa*

Like in §2.2, we denote by r_i the pixels' grey-level values of channel c_i in the NOAA–AVHRR acquisition dataset ($1 \leqslant i \leqslant 5$). Among the simplest functions that makes use of the c_2 and c_3 spectral bands, we simply take the sum $\varphi(c_2, c_3) = r_2 + r_3$ with the following conventions: first the values r_2 and r_3 are normalized between 0 and 1, and the result is clamped to 1 if $r_2 + r_3 > 1$. For the Genoa incident, the result is presented in figure 4. As the figure shows, the result is particularly good for this dataset: almost all clouds are eliminated, and the plume only remains, displaying strong contrast changes due to the aerosol's radiative and reflective properties encoded by spectral bands c_2 and c_3.

4.2 *Baghdad*

This dataset was recorded over Iraq during the 2003 war. It consists of eight temporal acquisitions. The seventh acquisition was operated at night, consequently

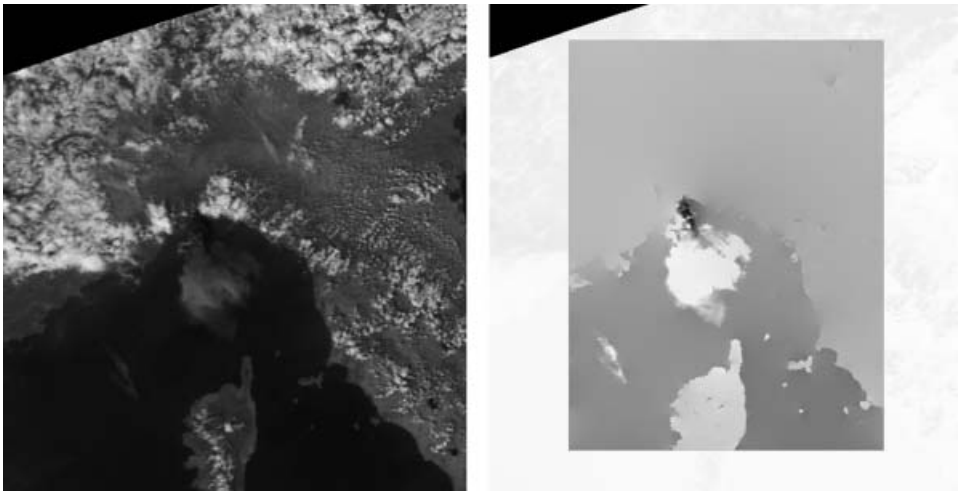

Figure 4. Left: the original signal, corresponding to the channel c_2 (near infrared), NOAA–AVHRR acquisition of the fire accident near Genoa (acquisition date: April, 13, 1991). Right: the resulting multispectral reduced signal computed on a selected area of the original dataset.

acquisitions in channels c_1 and c_2 are unavailable for the seventh dataset. The dataset records very clearly a huge plume over Baghdad, created by the explosions. The plume is rapidly changing in shape. We use the same φ function as in previous subsection. In figure 5, top, the c_2 channel of the first temporal acquisition is displayed. The plume is visible in the form of a dark streak below the centre of the image. The middle image shows the c_5 spectral band, which serves for the computation of the MSM. The resulting multispectral reduced signal is shown on the bottom image, with the plume clearly isolated, along with some water bodies. In figure 6 the multispectral reduced signals for temporal acquisitions 2, 3, 4, 5, 6 and 8 are shown. In these views, the changing shape of the plume is captured. The image corresponding to the eight temporal acquisition was very cloudy, hence demonstrating the power of the method.

4.3 *Fire events in Guadalajara, Spain*

The plume generated by the fire incidents in Spain is of a different nature from the two previous examples. Probably because of the presence of a dominant wind, the plume is very elongated, the turbulent behaviour of the temperature is not well recorded, and a reduced signal generated by a function $\varphi(c_2, c_3)=r_2+r_3$ does not produce satisfactory results. In that case, it is a better idea to simply rely on the temperature information itself, and use a simple function $\varphi(c_4)=r_4$ in conjunction with an MSM computed on the c_5 channel as before. We show the result in figure 7, which is also referred to in the comparison with the pixel-based algorithm, in §4.4.2. In this example, we performed the computation for the seventh acquisition only, as the other temporal acquisitions are recorded before the event. The plume is well visible on the resulting synthesized reduced signal, but clouds are also present at the bottom of the image. There is, however, a much greater variability in grey-level values for the pixels belonging to the plume (from white to grey), corresponding to higher differences in the recorded temperature values.

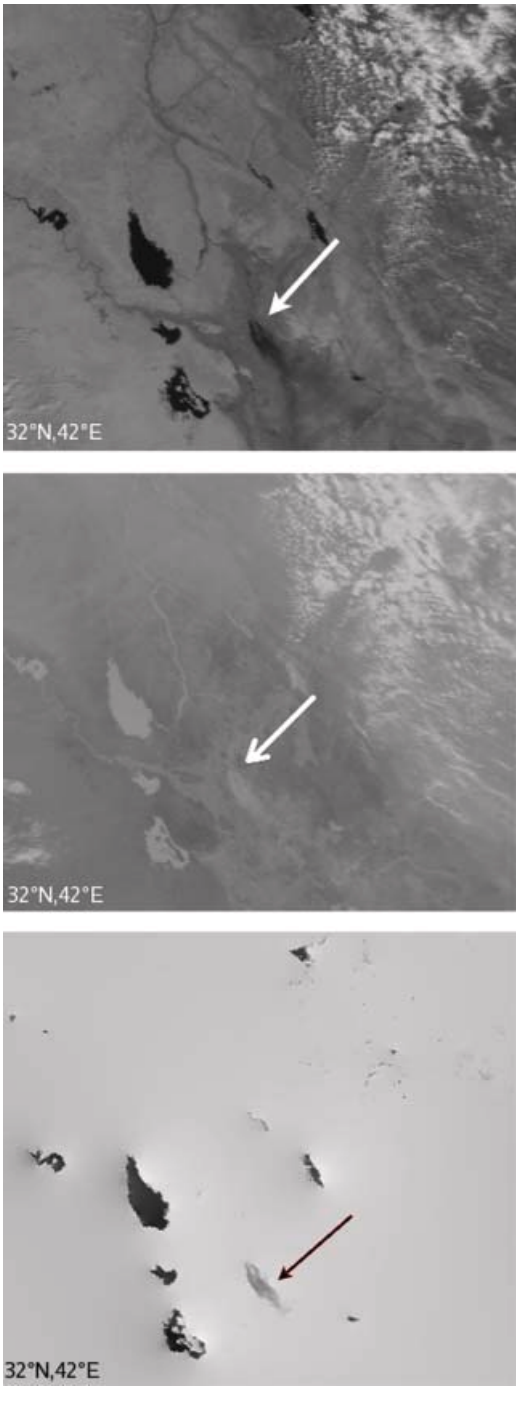

Figure 5. Top: NOAA–AVHRR channel c_2 in the first temporal acquisition, with the plume over Baghdad (white arrow). Different bodies are present: water, soil, clouds (note: coordinates are approximate). Middle: channel c_5 of the same temporal acquisition, (white arrow: plume). Bottom: the resulting multispectral reduced signal. The plume is clearly extracted, clouds are almost eliminated. The plume is indicated by the black arrow. Remains of cloudy pixels are present in the upper part.

Figure 6. Top row: synthesized multispectral reduced signals for the second, third and fourth temporal acquisitions (note: coordinates are approximate). Bottom row: synthesized multispectral reduced signals for the fifth, sixth and eighth temporal acquisitions (variable plume is indicated by arrow). The city of Baghdad is located as in figure 5, corresponding to the place pointed to by the arrow in the first image (top, left).

4.4 *Improvement of the pixel-based algorithm*

4.4.1 Review of the algorithm. The pixel-based algorithm, as described by Chrysoulakis and Cartalis (2003), makes use of the two indices NDVI and CLD (see §2.2, equation 1). These two indices define a two-dimensional feature space, intended to help the discrimination between plume pixels and other bodies (underlying surface, clouds, water bodies). A specific dataset of a fire accident that occurred in the Netherlands is used to calibrate the algorithm: using the spectral signatures of plumes, clouds, land surfaces and water surfaces, a threshold value of 0.85 is used for the discrimination between cloud and plume pixels with CLD. Then, assuming cloud pixels are masked, NDVI can be used to discriminate plume pixels from the underlying surface. NDVI, with the associated threshold value of 0, is used to mask pixel values corresponding to water bodies. On the two-dimensional feature space defined by NDVI and CLD, the relative positions of plumes, clouds, water bodies, land surfaces cover different areas. The sensibility to threshold values is a key aspect. An RGB image (CLD, NDVI, 0) is used to visualize the results. An error analysis and evaluation of the algorithm is introduced by measuring the overlapping percentage among the areas. Using mean values and standard deviations of pixels belonging to the different classes, ellipses centred on the different classes in the feature space are defined according to a probability level of 68.27%. It is found that the efficiency for the 'real event' detection is good, but the ability of the algorithm to

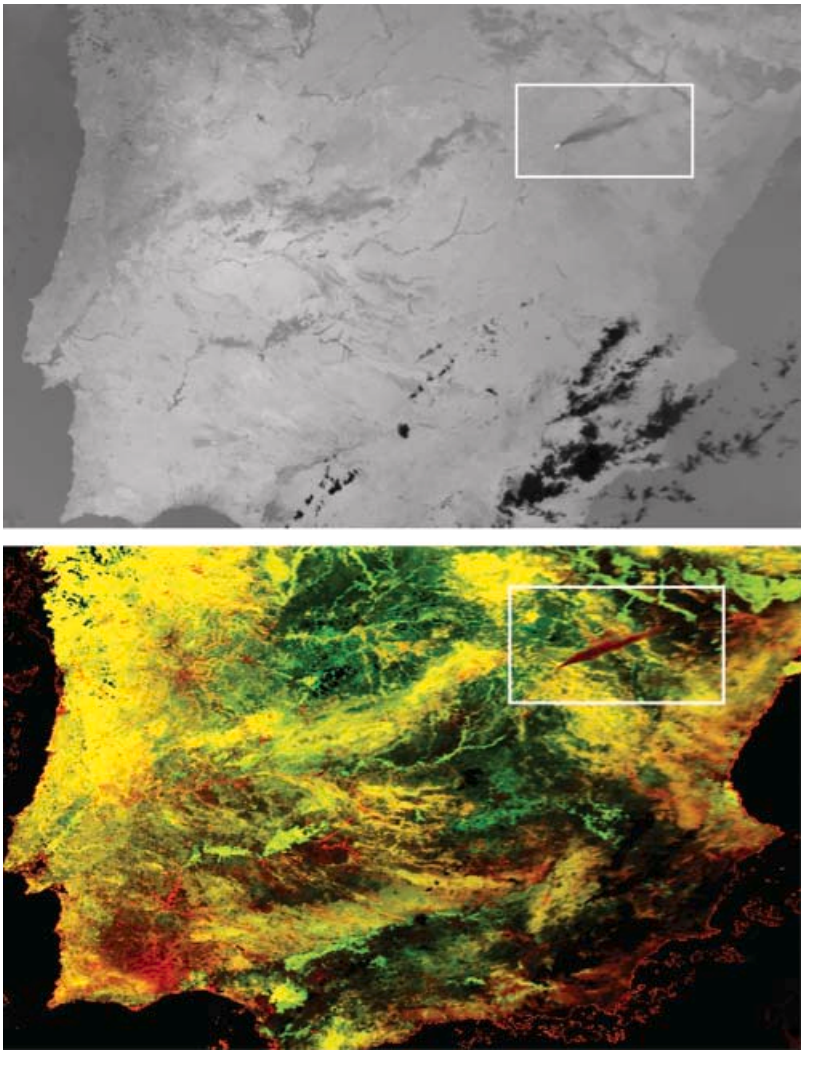

Figure 7. Top: the reduced signal for the seventh acquisition of the Spain dataset (plume inside white rectangle). We also display, in the bottom image, the result of the pixel-based algorithm introduced by Chrysoulakis and Cartalis (2003). The bottom consists of the RGB signal associated to (CLD, NDVI, 0). In this image, red-coloured pixels are plume pixels candidates.

reject 'false alarms' is reduced in certain cases. Moreover, the algorithm is threshold-dependent.

4.4.2 Improvement provided by the MMF. After the execution of the pixel-based algorithm, in the RGB image (CLD, NDVI, 0), plume pixels appear primarily as red-coloured. There are other red-coloured pixels, corresponding to the overlapping areas of the 2D feature space. We show the advantage of using the multispectral reduced signal in figure 7: instead of providing the pixel-based algorithm with the three NOAA–AVHRR data (c_1, c_2, c_5), one can use (c_1, c_2, p), with p being the multispectral reduced signal. From the reconstruction properties, signal p, which is

built on channel c_5'MSM, will alter CLD values mainly for some non-plume pixels: the plume is kept unchanged in p but an important part of the non-plume reddish pixels will not persist, since the reconstruction process produces for these pixels different grey-level values than the original ones in channel c_5.

4.4.3 Comments. The notion of multispectral reduced signal, which is derived from the reconstruction formula (5) in which we make use of the gradients coming from a functional defined on the grey-level values of a multispectral vector data, can considerably enhance the discrimination between plumes and other bodies (§§4.1–4.3). We propose to use it as a preprocessing step before the applications of the pixel-based algorithm reviewed in §2.2. Its main advantage, as a preprocessing step, comes from the following arguments:

- It reduces the dimensions of the histograms needed in the determination of thresholds values for the indices NDVI and CLD: indeed, as described by Chrysoulakis and Cartalis (2003) and Chrysoulakis *et al.* (2007), a fundamental step in the processing of the pixel-based algorithm is to operate the determination of thresholds from histogram data. This step is also crucial, because it is very sensitive to the size of the histograms and affects notably the global robustness of the pixel-based method. Using (in the form of input data) the synthesized multispectral reduced signal in the pixel-based algorithm provides less sensibility to histogram variations.
- It makes use of spectral band c_3, thus reducing the apparition of false alarms which come very often from low NDVI values: indeed, the pixel-based method did not make use of that channel, which contains physically-relevant information. The spectral band c_3 is used by other methods for fire detection (Li *et al.*, 2001).
- It makes the determination of 'universal' thresholds in the pixel-based algorithm easier because the reduced signal keeps the real values acquired in channels c_2, c_3 or c_4 (depending on the functional φ used). The reduced signal lowers the number of potential plume pixels and keeps real values acquired in multispectral bands in the reconstructed image. The advantage is clearly visible in all the result figures presented, and the enhancement is particularly noticeable for instance in figure 4 (right) where many non-plume pixels have been eliminated, while the turbulent behaviour of the plume is kept.

The pixel-based algorithm is given, as input, the synthesized multispectral reduced signals computed using the theory described above. The choice of the function φ, is not, at this moment, automatically determined. The various functions used in the examples produce different reduced signals which can be used as inputs to the pixel-based processing algorithm. A fundamental feature of the multispectral reduced signal is that it makes use of the gradients of the pixels' grey-level values in the different bands, and restores the distribution function of the physical values recorded in the bands, without performing any equalization that would lose the physical distribution function of the acquired signal. In consequence, the reduced signal offers a smaller training set of pixels whose grey-level values are used in the threshold determination process.

The problem of finding a satisfactory *universal synthesized multispectral* reduced signal (i.e. a unique function φ that would handle the case of a large class of NOAA–AVHRR datasets) is not easy. In this study, we make use of two such

reduced signals. But the use of multiple synthesized multispectral signals does not add significant overhead.

5. Conclusion

In this work an important enhancement of the pixel-based algorithm presented in §2.2 is introduced. It consists in reducing the set of potential plume pixels by analysing the spatial distribution of grey-level values in the framework of the microcanonical multifractal formalism (MMF). The MMF introduces a powerful method for deriving values of singularity exponents associated to the multifractal measure whose density is defined by the norm of the signal gradient. From the singularity exponents, the hierarchy of supergeometric structures associated to a turbulent geophysical flow is derived; among these structures, the Most Singular Manifold (MSM), defined as the set of pixels having the sharpest transitions, can be used to reconstruct the signal entirely, even in the case of Fully Developed Turbulence (or FDT).

Consequently, the research presented in this study hinges on the ability of the MSM to encode the turbulent character of various geophysical fluid flows, likes plumes or clouds, and on a reconstruction formula that makes use of the multispectral information provided by a NOAA–AVHRR acquisition dataset; the reconstruction formula restores the physical values of any combination of the different multispectral acquisitions of a signal along the most relevant streamlines (turbulent areas) detected from the temperature distribution function (infrared band c_5). It allows the derivation of a synthetic multispectral reduced signal computed by performing a diffusion of multispectral grey-level values given in a NOAA–AVHRR acquisition dataset along the MSM computed in the c_5 band. The reduced signal considerably reduces the set of potential plume pixels and keeps the distribution function of the acquired bands inside the spatial area defined by the plumes. Consequently, the reduced signal can be used as inputs for the pixel-based algorithm, and considerably enhances the discrimination process in the determination of plume pixels. It also eases the determination of universal thresholds in the pixel-based algorithm.

Acknowledgement

This work was done in the framework of the PLUMESAT project ('Use of a satellite ground receiving station for the detection and monitoring of fires and plumes caused by major natural and man-made disasters'). The PLUMESAT project is funded by:

- The 'Competitveness' Programme, Action 4.3.6.1.γ of the General Secretary of Research and Technology of the Ministry of Development of Greece.
- The 'Platon 2005' Integrated Action Programme (PAI) of the French Ministry of Foreign Affairs, through EGIDE.

References

Arneodo, A., Argoul, F., Bacry, E., Elezgaray, J. and Musy, J.F., 1995, *Ondelettes, Multifractales et Turbulence* (Paris: Diderot Editeur).

Cahoon Jr., D., Stocks, R., Levine, B.J., Coffer III, W.R. and Pierson, J.M., 1994, Satellite analysis of the severe 1987 forest fires in Northern China and Southearstern Siberia. *Journal of Geophysical Research*, **99**, pp. 18627–18638.

CRISTOPHER, S.A., KICHE, D.V., CHOU, J. and WELCH, R.M., 1996, First estimates of the radiative forcing of aerosols generated from biomass burning using satellite data. *Journal of Geophysical Research – Atmospheres*, **101**, pp. 21265–21273.

CRYSOULAKIS, N. and CARTALIS, C., 2003, A new algorithm for the detection of plumes caused by industrial accidents, based on NOAA/AVHRR imagery. *International Journal of Remote Sensing*, **24**, pp. 3353–3367.

CRYSOULAKIS, M. and OPIE, C., 2004, Using NOAA and FY imagery to track plumes caused by the 2003 bombing of Baghdad. *International Journal of Remote Sensing*, **25**, pp. 5247–5254.

CRYSOULAKIS, N., HERLIN, I., PRASTACOS, P., YAHIA, H., GRAZZINI, J. and CARTALIS, C., 2007, An improved algorithm for the detection of plumes caused by technological hazards using NOAA/AVHRR imagery. *Remote Sensing of Environment*, **108**, pp. 393–406.

CHU, D.A., KAUFMAN, Y.J., REMER, L.A. and HOLBEN, B.N., 1998, Remote sensing of smoke from MODIS airborne simulator during the SCAR-B experiment. *Journal of Geophysical Research*, **18**, pp. 31979–31988.

FLASSE, S.P. and CECCATO, P., 1996, A contextual algorithm for AVHRR fire detection. *International Journal of Remote Sensing*, **17**, pp. 419–424.

FRISCH, U., 1995, *Turbulence, The Legacy of Kolmogorov* (Cambridge: Cambridge University Press).

GRAZZINI, J., TURIEL, A. and YAHIA, H., 2006, Multifractal formalism for remote sensing: A contribution to the description and the understanding of meteorological phenomena in satellite images. In *Fractal 2006*, Vol. 2, M.N. Novak (Ed.) (Singapore: World Scientific Publishing), pp. 247–256.

GRAZZINI, J., TURIEL, A. and YAHIA, H., 2002, Entropy estimation and multiscale processing in meteorological satellite images. *Proceedings of the International Conference on Pattern Recognition*, **3**, pp. 764–768.

HASHIM, M., KANNIAHL, K.D., AHMAD, A., RASIB, A.W. and IBRAHIM, A.L., 2004, The use of AVHRR data to determine the concentration of visible and invisible tropospheric pollutants originating from a 1997 forest fire in Southeast Asia. *International Journal of Remote Sensing*, **25**, pp. 4781–4794.

LI, Z., KAUFMANN, Y.J., ICHOKU, C., FRASER, R., TRISCHENKO, A., GIGLIO, L., JIN, J. and YU, X., 2001, A review of AVHRR-based active fire detection algorithms: principles, limitations, and recommendations. In *Global and Regional Vegetation Fire Monitoring from Space: Planning and Coordinated International Effort*, F. Ahern, J.G. Goldammer and C. Justice (Eds) (The Hague: SPB Academic Publishing), pp. 199–225.

PARISI, G. and FRISCH, U., 1985, A multifractal model of intermittency. In *Turbulence and Predictability in Geophysical Fluids Dynamics and Climate Dynamics*, Proceedings of the International School of Physics, E. Fermi, M. Ghil, R. Benzhi, and G. Parisi (Eds.) (Amsterdam: North-Holland), pp. 84–88.

ROUX, A., ARNÉODO, A. and DCOSTER, N., 2000, A wavelet-based method for multifractal image analysis III: Applications to high resolution satellite images of cloud structures. *European Physical Journal*, **B**, pp. 765–786.

SCHERTZER, D. and LOVEJOY, S., 1997, Universal multifractal do exist: Comments on 'A statistical analysis of mesoscale rainfall as a random cascade'. *Journal of Applied Meteorology*, **36**, pp. 1296–1303.

SHE, A. and LEVÊQUE, E., 1994, Universal scaling laws in fully developped turbulence. *Physical Review Letters*, **72**, pp. 336–339.

TURIEL, A. and PARGA, N., 2000, The multifractal structure of contrast changes in natural images: From sharp edges to textures. *Neural Computing*, **12**, pp. 763–793.

TURIEL, A. and DEL POZO, A., 2002, Reconstructing images from their most singular fractal manifold. *IEEE Transactions on Image Processing*, **11**, pp. 345–350.

TURIEL, A., GRAZZINI, J. and YAHIA, H., 2005a, Multiscale techniques for the detection of precipitation using thermal IR satellite images. *IEEE Geoscience and Remote Sensing Letters*, **2**, pp. 447–450.

TURIEL, A., ISERN-FONTANET, J., GARCIA-LADONA, E. and FONT, J., 2005b, Multifractal method for the inst. eval. of the stream function in geophysical flows. *Physical Review Letters*, **95**, p. 10450.